Efficient multiscale magnetic-domain analysis of iron-core material under mechanical stress

AUTHOR(S):

Nishikubo, Atsushi; Ito, Shumpei; Mifune, Takeshi; Matsuo, Tetsuji; Kaido, Chikara; Takahashi, Yasuhito; Fujiwara, Koji

CITATION:

Nishikubo, Atsushi ...[et al]. Efficient multiscale magnetic-domain analysis of iron-core material under mechanical stress. AIP Advances 2017, 8(5): 056617.

ISSUE DATE:

2017-12-22

URL:

http://hdl.handle.net/2433/235619

AIP ADVANCES **8**, 056617 (2018)

Efficient multiscale magnetic-domain analysis of iron-core material under mechanical stress

Atsushi Nishikubo,[1] Shumpei Ito,[1] Takeshi Mifune,[1] Tetsuji Matsuo,[1,a]
Chikara Kaido,[2] Yasuhito Takahashi,[3] and Koji Fujiwara[3]
[1]*Kyoto University, Kyotodaigaku-katsura, Nishikyo-ku, Kyoto 615-8510, Japan*
[2]*National Institute of Technology, Kitakushu College, Kitakushu 802-0985, Japan*
[3]*Doshisha University, 1-3, Tatara Miyakodani, Kyotanabe, Kyoto 610-0321, Japan*

(Presented 7 November 2017; received 29 September 2017; accepted 6 November 2017;
published online 22 December 2017)

For an efficient analysis of magnetization, a partial-implicit solution method is improved using an assembled domain structure model with six-domain mesoscopic particles exhibiting pinning-type hysteresis. The quantitative analysis of non-oriented silicon steel succeeds in predicting the stress dependence of hysteresis loss with computation times greatly reduced by using the improved partial-implicit method. The effect of cell division along the thickness direction is also evaluated.
https://doi.org/10.1063/1.5007005

I. INTRODUCTION

The magnetic degradation of core materials through mechanical stress[1–3] has been intensively studied recently because of the deterioration in motor performance it causes. However, measuring the stress-dependent property under arbitrary combinations of magnetization and stress directions is difficult in practice. Physical model of magnetization[4–7] is accordingly required to predict the stress-dependent magnetic property from minimal magnetic measurements. The assembled-domain structure model (ADSM)[7,8] is one such model that includes the magneto-mechanical interaction and the effects of pinning[8,9] in the crystal-grain scale. Being a multiscale model, the macroscopic magnetization is constructed by assembling mesoscopic unit cells. For non-oriented (NO) silicon steel, the ADSM successfully predicts the increase in hysteresis loss arising from compressive stress.[9]

In NO silicon steel, the multiple-grain structure is observed along the normal direction (ND) (or sheet-thickness direction), where surface magnetic poles affect the magnetic-domain behavior. To reveal the effect of surface poles on the magnetization property of a core material, the multiple-grain structure has to be represented by the ADSM having cell division along the ND. However, further cell division incurs large computational costs.

To accelerate the energy-minimization process for the ADSM, a partial-implicit scheme was proposed,[10] where the Jacobian matrix is reduced to a block-diagonal matrix to avoid full matrix inversions. This partial-implicit scheme revealed the magnetization transition observed in a giant magneto-impedance thin-film element by configuring an assembly of two-domain mesoscopic cells based on the induced uniaxial anisotropy of the thin film. To treat the cubic anisotropy, the analysis of silicon steel requires six-domain mesoscopic cells, which increases the size of the diagonal blocks in the Jacobian matrix and consequently requires extensive computations to execute the partial implicit scheme. In addition, an efficient loss analysis requires the pinning field to be included in the partial-implicit scheme. This paper improves the partial-implicit scheme for the ADSM using six domain cells that exhibit pinning-type hysteresis. An analysis of the stress-dependent loss in silicon steel is given demonstrating the efficiency of the improved scheme. The effect of cell division along the ND is also evaluated.

[a]Electronic mail: matsuo.tetsuji.5u@skyoto-u.ac.jp

II. PARTIAL–IMPLICIT SCHEME FOR ADSM WITH PINNING FIELD

A. ADSM

The ADSM is constructed by assembling mesoscopic cells called simplified domain structure models (SDSMs) (Fig. 1). Depending on whether the anisotropy is unidirectional or cubic, each cell of the SDSM has two or six domains. The analysis of silicon steel requires six-domain cells,[7] where the magnetization state in each cell is represented by the volume ratios r_i and the magnetization vectors $\boldsymbol{m}_i = (\sin\theta_i\cos\phi_i, \sin\theta_i\sin\phi_i, \cos\theta_i)$ $(i = 1,\ldots, 6)$. The variable vector in a cell j is denoted $\boldsymbol{x}_j = (\theta_{1,j}, \ldots, \theta_{6,j}, \phi_{1,j}, \ldots, \phi_{6,j}, r_{1,j}, \ldots, r_{5,j})$ where $r_{6,j} = 1 - r_{1,j} \ldots - r_{5,j}$. The magnetization state is determined by finding a set of variable vectors $\boldsymbol{x}_j$ $(j = 1, 2, \ldots)$ that gives a local minimum for the total magnetic energy e comprising contributions from, for example, the Zeeman energy, crystalline anisotropy energy, magnetostatic energy, and magnetoelastic energy.

The local minimization of e is achieved by solving the ordinary differential equations (ODEs) given by

$$\frac{d\boldsymbol{X}}{dt} = \boldsymbol{Y}, \qquad \frac{d\boldsymbol{Y}}{dt} = -\frac{\partial e}{\partial \boldsymbol{X}} - \beta\boldsymbol{Y} = \boldsymbol{F}(\boldsymbol{X}) - \beta\boldsymbol{Y}, \tag{1}$$

where $\boldsymbol{X} = (\boldsymbol{x}_1, \boldsymbol{x}_2, \ldots)$, $\boldsymbol{F}(\boldsymbol{X}) = -\partial e/\partial \boldsymbol{X}$, β is the coefficient of dissipation, and $\boldsymbol{Y}$ is an intermediate variable vector. Equation (1) is an artificial state equation for $\boldsymbol{X}$ and $\boldsymbol{Y}$, where the time t has no physical meaning. A local energy minimum is obtained by numerically integrating Eq. (1) until reaching an equilibrium point where $d\boldsymbol{X}/dt = d\boldsymbol{Y}/dt = 0$. This method of solution can be regarded as a gradient-descent method with a momentum.[11]

B. Partial-implicit scheme

To solve stiff ODEs, the forward Euler method often induces numerical instability unless a very small time-step is used. An implicit scheme such as the backward Euler method is effective for the stable time-marching. The implicit time-integration of (1) requires the Hessian matrix $\partial^2 e/\partial \boldsymbol{X}^2$ in the Jacobian Matrix. However, the Hessian matrix becomes dense because of the magneto-static dipole–dipole interaction between all cells. When the number of cells is large, the calculation of such matrices requires large computation times because the nonlinear solution by the Newton–Raphson (NR) iteration needs to invert the Jacobian matrix including the Hessian matrix.

The partial-implicit scheme[10] partitions the magnetostatic field $\boldsymbol{h}(j)$ in cell j into a near field $\boldsymbol{h}_{\mathrm{stin}}(j)$ and far field $\boldsymbol{h}_{\mathrm{stex}}(j)$, where $\boldsymbol{h}_{\mathrm{stin}}(j)$ and $\boldsymbol{h}_{\mathrm{stex}}(j)$ are generated by cell j and by the other cells, respectively. The far field is temporally integrated by an explicit scheme whereas the near field is processed by an implicit scheme. The partial-implicit time integration scheme is written as

$$\boldsymbol{X}^{n+1} = \boldsymbol{X}^n + \Delta t\boldsymbol{Y}^{n+1}, \quad \boldsymbol{Y}^{n+1} = \boldsymbol{Y}^n + \Delta t\boldsymbol{F}_{\mathrm{im}}(\boldsymbol{X}^{n+1}) + \Delta t\boldsymbol{F}_{\mathrm{ex}}(\boldsymbol{X}^n) - \Delta t\beta\boldsymbol{Y}^{n+1}, \tag{2}$$

where Δt is the time-step and n is the time-index; $\boldsymbol{F}$ is decomposed as $\boldsymbol{F}(\boldsymbol{X}) = \boldsymbol{F}_{\mathrm{im}}(\boldsymbol{X}) + \boldsymbol{F}_{\mathrm{ex}}(\boldsymbol{X})$; $\boldsymbol{h}_{\mathrm{stex}}$ is included in $\boldsymbol{F}_{\mathrm{ex}}$, and all the other terms of $\boldsymbol{F}$ are included in $\boldsymbol{F}_{\mathrm{im}}$. The nonlinear equation (2) for $(\boldsymbol{X}, \boldsymbol{Y})$ is solved using the NR method. The Jacobian matrix $\boldsymbol{J}_{XY}$ used in the NR iteration is block diagonal consisting of cell blocks given as

$$\boldsymbol{J}_{XY}(\boldsymbol{X}, \boldsymbol{Y}) = \mathrm{blockdiag}\{\boldsymbol{J}_{xy1}, \boldsymbol{J}_{xy2}, \cdots\}, \tag{3}$$

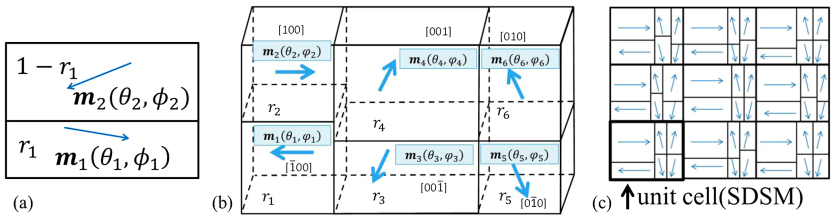

FIG. 1. ADSM: (a) mesoscopic two-domain particle, (b) mesoscopic six-domain particle, and (c) assembly of mesoscopic particles.

$$\boldsymbol{J}_{xyj} = \begin{pmatrix} \mathbf{1} & -\Delta t\mathbf{1} \\ -\Delta t \dfrac{\partial \boldsymbol{f}_{\mathrm{im}j}}{\partial \boldsymbol{x}_j} & (1+\beta\Delta t)\mathbf{1} \end{pmatrix}, \boldsymbol{F}_{\mathrm{im}} = \begin{pmatrix} \boldsymbol{f}_{\mathrm{im}1} \\ \boldsymbol{f}_{\mathrm{im}2} \\ \vdots \end{pmatrix}, \tag{4}$$

where j is the cell number and $\mathbf{1}$ is the 17×17 unit matrix. The NR iteration is performed cell-by-cell. To avoid the inversion of the 34×34 matrix (4), this paper presents a method to reduce the matrix size.

By substituting $\boldsymbol{Y}^{n+1} = (\boldsymbol{X}^{n+1} - \boldsymbol{X}^n) / \Delta t$ into the second equation of (2), $\boldsymbol{Y}^{n+1}$ can be eliminated,

$$\boldsymbol{G}(\boldsymbol{X}^{n+1}) = (\beta + \frac{1}{\Delta t})(\boldsymbol{X}^{n+1} - \boldsymbol{X}^n) - \boldsymbol{Y}^n - \Delta t\boldsymbol{F}_{\mathrm{im}}(\boldsymbol{X}^{n+1}) - \Delta t\boldsymbol{F}_{\mathrm{ex}}(\boldsymbol{X}^n) = 0 \tag{5}$$

The partial-implicit scheme proceeds by solving Eq. (5) with the NR method cell-by-cell, where the size of the matrix consisting of the block-diagonal Jacobian matrix is reduced to 17×17 as

$$\boldsymbol{J}_X = \frac{\partial \boldsymbol{G}(\boldsymbol{X}^{n+1})}{\partial \boldsymbol{X}^{n+1}} = \mathrm{blockdiag}\{\boldsymbol{J}_{x1}(\boldsymbol{x}_1^{n+1}), \boldsymbol{J}_{x2}(\boldsymbol{x}_2^{n+1}), \cdots\}, \tag{6}$$

$$\boldsymbol{J}_{xj}(\boldsymbol{x}_j) = (\beta + \frac{1}{\Delta t})\mathbf{1} - \Delta t \frac{\partial \boldsymbol{f}_{\mathrm{im}j}}{\partial \boldsymbol{x}_j}. \tag{7}$$

C. Pinning field

In the presence of pinning sites, the pinning field h_{p} is additionally required cell by cell to change the volume ratio $r_{j,i}$ in a cell j involved in the domain wall motion.[8] The energy minimization procedure uses terms of $-\partial e/\partial r_{j,i}$ to decrease e by changing $r_{j,i}$. To include the pinning effect, the pinning energy e_{p} in every cell is added to e, where $\partial e_{\mathrm{p}}/\partial r_{j,i}$ is the pinning field h_{p} in cell j. In other words, the effective field $-\partial e_{\mathrm{p}}/\partial r_{j,i}$ represents the force of friction acting on the domain wall. The pinning field caused by the wall motion of domain i in cell j is given as $h_{\mathrm{p}} = h_{\mathrm{p}}(2r_{j,i} - 1)$. Thus, $\partial e_{\mathrm{p}}/\partial r_{j,i}$ is expressed as

$$\partial e_{\mathrm{p}}/\partial r_{j,i} = 2h_{\mathrm{p}}(2r_{j,i} - 1) = S(2r_{j,i} - 1). \tag{8}$$

where S is a hysteretic function described by the stop model.[8,9] Terms $\partial e_{\mathrm{p}}/\partial \phi_{j,i}$ and $\partial e_{\mathrm{p}}/\partial \theta_{j,i}$ are set to zero.

The stop model[12] specifies

$$S(m) = \sum_{n=1}^{N\mathrm{s}} g_n(s_n(m)), \tag{9}$$

where N_{s} is the number of stop hysterons and g_n is the single-valued function called the shape function. The stop hysteron $s_n(m)$ is given as

$$s_n(m) = \max(\min(m - m^0 + s_n^0, \eta_n), -\eta_n), \tag{10}$$

where $(m^0, s_n{}^0)$ is the values of (m, s_n) at the previous time point, and η_n is a positive constant giving the height of the n-th stop hysteron. The shape functions g_n are identified from the MH loops generated by the pinning model.

The term in Eq. (8) is included in $\boldsymbol{F}_{\mathrm{im}}(\boldsymbol{X})$, which requires the derivative of $\partial S(m)/\partial m$ to calculate $\partial^2 e_{\mathrm{p}}/\partial r_{j,i}{}^2$, specifically,

$$\frac{\partial^2 e_{\mathrm{p}}}{\partial r_{j,i}^2} = 2S'(2r_{j,i} - 1), \tag{11}$$

$$S'(m) = \frac{\partial S(m)}{\partial m} = \sum_{n=1}^{N\mathrm{s}} \frac{\partial g_n(s_n)}{\partial s_n} \frac{\partial s_n(m)}{\partial m}, \tag{12}$$

$$\frac{\partial s_n(m)}{\partial m} = \begin{cases} 1 & (|m - m^0 + s_n^0| < \eta_n) \\ 0 & (|m - m^0 + s_n^0| \geq \eta_n) \end{cases}. \tag{13}$$

III. COMPUTATIONAL RESULTS

A. Speed-up by partial-implicit method

For simulations of the magnetization of a NO silicon steel sheet, the anisotropy constant for cubic anisotropy is $K = 3.8 \times 10^4$ J/m^3, the magnetostriction constants are $\lambda_{100} = 2.7 \times 10^{-5}$, $\lambda_{111} = -1.0 \times 10^{-5}$, which are typical values for 2-3 % Si-Fe,[4,13] and $\mu_0 M_S = 2.2$ T. The density function of pinning sites is given by a Gaussian distribution.

The procedure begins by first dividing the rolling direction (RD), transverse direction (TD), and ND into $8 \times 8 \times 1$ cells, where the unit cell dimension ratio is 1: 1: 10^{-4} and the crystal orientations in the 64 cells are randomly distributed. Figure 2 compares the simulated MH loops and computation time using the explicit and partial-implicit schemes. The computation times were taken for a magnetization sequence of $\mu_0 M = 0$ T (demagnetized) $\rightarrow$ 1.7 T $\rightarrow$ −1.7 T with 120 steps. The partial-implicit scheme obtains almost the same MH loops as the explicit scheme. The explicit scheme often leads to numerical instability if the time-step is more than 0.01. The partial-implicit scheme achieves a stable energy minimization with time-step 0.3. As a result the partial-implicit scheme can greatly reduce computation times with and without the compressive mechanical stress [see Fig. 2(b)].

B. Cell division along normal direction

To examine the effect of cell division along the ND, the RD, TD, and ND are divided into $8 \times 1 \times 8$ cells. The stress dependent magnetic property of steel sheet was measured with a stress-loading single sheet tester,[14] where a strip sample was attached with a glass epoxy plate to prevent buckling; one end of the sample was fixed and the other end was pushed/pulled mechanically. Every measurement was performed once per measuring condition because our preliminary check under several conditions showed that the reproducibility of stress-dependent measurement was almost as

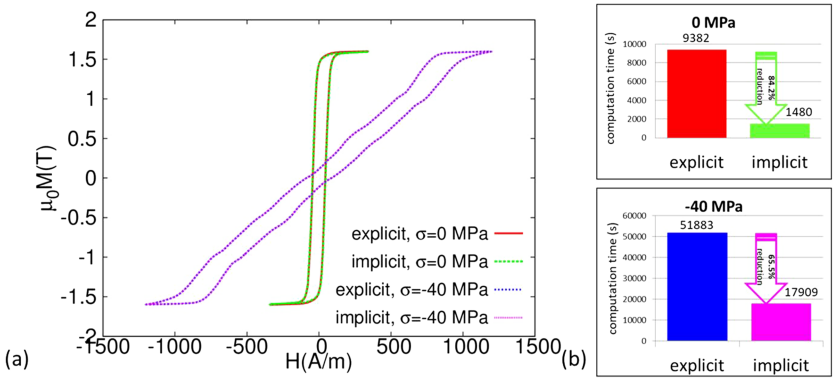

FIG. 2. Results obtained by explicit and partial-implicit schemes: (a) M-H loops and (b) reduction in computation times.

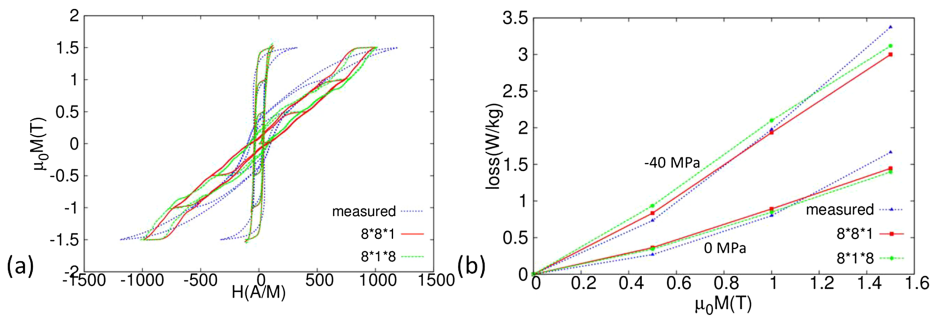

FIG. 3. Results obtained by a cell-division of $8 \times 8 \times 8$ and $8 \times 1 \times 8$: (a) M-H loops and (b) hysteresis loss (50 Hz).

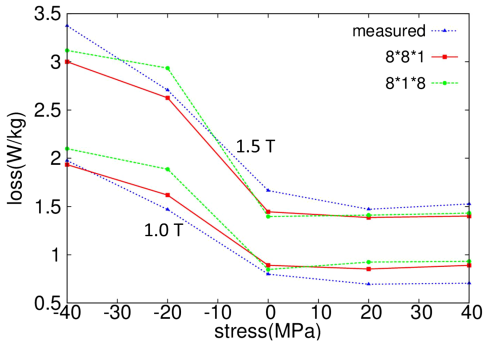

FIG. 4. Stress dependence of hysteresis loss (50 Hz).

good as the stress-free measurement. From the simulated hysteresis loss with and without mechanical stress along the RD (Fig. 3), the loss increase under compressive stresses is quantitatively predicted by the ADSM, where the compressive stress suppresses the development of magnetic domains having magnetizations nearly parallel to the stress direction and hence increases the pinning field.[9] From the dependence of hysteresis loss on the applied stress along the RD (Fig. 4), the division along the ND does not greatly affect the loss. This is probably because the demagnetizing field along the ND is too large for surface magnetic poles to appear in the simulation. The mesoscopic modeling using the average magnetization should be improved to examine the effect of surface poles.

IV. CONCLUSION

For ADSM, the partial-implicit method greatly reduced computation times in the magnetization analysis, thereby enabling a large-scale analysis with cell division along the ND. The accuracy of magnetization analysis may be improved by more detailed modeling including local magneto-mechanical interactions[4] and surface charges.

ACKNOWLEDGMENTS

This work was supported in part by the Japan Society for the Promotion of Science under Grant-in-Aid for Scientific Research (C) Grant No. 17K06300. We thank Richard Haase, Ph.D, from Edanz Group (www.edanzediting.com/ac) for editing a draft of this manuscript.

[1] M. LoBue, C. Sasso, V. Basso, F. Fiorillo, and G. Bertotti, "Power losses and magnetization process in Fe-Si non-oriented steels under tensile and compressive stress," J. Magn. Magn. Mater. **215-216**, 124–126 (2000).
[2] C. Kaido, N. Hirose, S. Iwasa, T. Hayashi, and Y. Waki, "Stress dependence of magnetic properties in non-oriented electrical steel sheets," J. Magn. Soc. Jpn. **34**, 140–145 (2010).
[3] Y. Kai, Y. Tsuchida, T. Todaka, and M. Enokizono, "Influence of stress on vector magnetic property under alternating magnetic flux conditions," IEEE Trans. Magn. **47**, 4344–4347 (2011).
[4] O. Hubert and L. Daniel, "Multiscale modeling of the magneto-mechanical behavior of grain-oriented silicon steels," J. Magn. Magn. Mater. **320**, 1412–1422 (2008).
[5] J. Fujisaki, A. Furuya, Y. Uehara, K. Shimizu, H. Oshima, T. Sasayama, and N. Takahashi, "Hysteresis modeling of a non-oriented electrical steel sheet under compressive stress," Proc. Joint Tech. Meeting Static App. Rotating Mach., SA-13–72/RM-13-86 (2013).
[6] L. Daniel, M. Rekik, and O. Hubert, "A multiscale model for magneto-elastic behaviour including hysteresis effects," Arch. Appl. Mech. **84**, 1307–1323 (2014).
[7] S. Ito, T. Mifune, T. Matsuo, and C. Kaido, "Macroscopic magnetization modeling of silicon steel sheets using an assembly of six-domain particles," J. Appl. Phys. **117**, 17D126 (2015).
[8] S. Ito, T. Mifune, T. Matsuo, C. Kaido, Y. Takahashi, and K. Fujiwara, "Domain structure model including pinning effect based on the statistical distribution function," IEEJ Trans. F.M. (accepted for publication).
[9] S. Ito, T. Mifune, T. Matsuo, C. Kaido, Y. Takahashi, and K. Fujiwara, "Simulation of the stress dependence of hysteresis loss using an energy-based domain model," AIP Advances **8**, 047501 (2018).
[10] S. Tejima, S. Ito, T. Mifune, T. Matsuo, and T. Nakai, "Partially-implicit method for fast magnetization analysis using assembled domain structure model," IEEE Trans. Magn. **53**, 7300404 (2017).
[11] N. Qian, "On the momentum term in gradient descent learning algorithms," Neural Networks **12**, 145–151 (1999).

[12] T. Matsuo and M. Shimasaki, "Isotropic vector hysteresis represented by superposition of stop hysteron models," IEEE Trans. Magn. **37**, 3357–3361 (2001).
[13] S. Chikazumi, *Physics of Ferromagnetism* (Oxford University Press, Oxford, 1997), p. 363.
[14] N. Kurita, Y. Takahashi, K. Fujiwara, and Y. Ishihara, "Magnetic field analysis taking account of stress-dependent magnetic properties of non-oriented electrical steel sheets," Proc. 18th COMPUMAG, Sydney, Australia (2011) PD7.7.